Multi-Step Fibrinogen Binding to the Integrin αIIbβ3 Detected Using Force Spectroscopy

Rustem I. Litvinov,* Joel S. Bennett,† John W. Weisel,* and Henry Shuman‡
*Department of Cell and Developmental Biology, †Hematology-Oncology Division of the Department of Medicine, and ‡Department of Physiology, University of Pennsylvania School of Medicine, Philadelphia, Pennsylvania

ABSTRACT The regulated ability of integrin αIIbβ3 to bind fibrinogen plays a crucial role in platelet aggregation and hemostasis. We have developed a model system based on laser tweezers, enabling us to measure specific rupture forces needed to separate single receptor-ligand complexes. First of all, we performed a thorough and statistically representative analysis of nonspecific protein-protein binding versus specific αIIbβ3-fibrinogen interactions in combination with experimental evidence for single-molecule measurements. The rupture force distribution of purified αIIbβ3 and fibrinogen, covalently attached to underlying surfaces, ranged from ~20 to 150 pN. This distribution could be fit with a sum of an exponential curve for weak to moderate (20–60 pN) forces, and a Gaussian curve for strong (>60 pN) rupture forces that peaked at 80–90 pN. The interactions corresponding to these rupture force regimes differed in their susceptibility to αIIbβ3 antagonists or Mn^{2+}, an αIIbβ3 activator. Varying the surface density of fibrinogen changed the total binding probability linearly >3.5-fold but did not affect the shape of the rupture force distribution, indicating that the measurements represent single-molecule binding. The yield strength of αIIbβ3-fibrinogen interactions was independent of the loading rate (160–16,000 pN/s), whereas their binding probability markedly correlated with the duration of contact. The aggregate of data provides evidence for complex multi-step binding/unbinding pathways of αIIbβ3 and fibrinogen revealed at the single-molecule level.

INTRODUCTION

The ability of integrins to interact with macromolecular ligands can be regulated by agonist-induced transmembrane signaling (1,2). Thus, the integrin αIIbβ3 on the surface of unstimulated platelets has a negligible affinity for soluble fibrinogen, but readily binds fibrinogen when platelets are stimulated by agonists such as adenosine diphosphate (ADP) and thrombin. Although there has been recent progress in understanding the mechanism of integrin regulation (3), a number of fundamental issues about ligand binding to integrins remain to be clarified (4). For example, the location and even the number of fibrinogen-binding sites on the αIIbβ3 molecule are uncertain (5). Moreover, kinetic studies suggest that the αIIbβ3-fibrinogen interaction is at least biphasic (6–8), implying that the binding and unbinding pathways between αIIbβ3 and fibrinogen are complex.

The information obtained from conventional receptor-ligand binding studies that make use of large ensembles of molecules or whole cells can be substantially enhanced when the studies are performed at the single-molecule level (9). This is now possible because of the development of new biophysical approaches, including atomic force microscopy (AFM) (10), surface force apparatus (11–13), micropipette suction technique (14), and the use of hydrodynamic flow (15). Several of these methods can measure the rupture forces between individual integrin molecules and their ligands, including fibrinogen (6,16–19).

We have developed a model system based on laser tweezers that is suitable for measuring the forces required to separate single ligand-receptor pairs (rupture forces) using either purified proteins or intact living cells. The technique of optically trapping and manipulating small particles using a focused laser beam, called laser tweezers, has become a valuable tool in molecular and cellular biology (20,21). Because the position of a particle can be determined precisely, laser tweezers can measure external forces applied to the particle with extremely high resolution (22,23). Accordingly, the technique has been used to measure the rigor bond strength between actin and heavy meromyosin (24,25) or α-actinin (26), protein A binding to immunoglobulin G (27), and P- and L-selectins binding to PSGL-1 (28). However, none of these studies analyzed the stochastic force spectra produced in many repeated receptor-ligand binding/unbinding cycles.

We used laser tweezers to study fibrinogen binding to either purified αIIbβ3 or αIIbβ3 on the surface of living platelets and concluded that there are two states of αIIbβ3 activation, inactive and active (29). Nonetheless, further analysis of the forced unbinding of fibrinogen from αIIbβ3 revealed unique features of this receptor-ligand pair. To increase the credibility and significance of the conclusions, we performed a thorough and statistically representative analysis of nonspecific protein-protein binding versus specific αIIbβ3-fibrinogen interactions in combination with experimental evidence for single-molecule measurements. Here we provide evidence that yield force histograms of individual

Submitted February 24, 2005, and accepted for publication June 20, 2005.

Address reprint requests to Henry Shuman, Dept. of Physiology, University of Pennsylvania School of Medicine, 601 Goddard Labs, 3710 Hamilton Walk, Philadelphia, PA 19104-6085. Tel.: 215-573-2757; Fax: 215-898-2653; E-mail: shuman@mail.med.upenn.edu.

0006-3495/05/10/2824/11 $2.00

doi: 10.1529/biophysj.105.061887

αIIbβ3-fibrinogen interactions display at least two different components that differ in kinetics, loading rate dependence, and susceptibility to inhibition or activation. Thus, our data suggest that although αIIbβ3 has only one state capable of interacting with its ligands, fibrinogen binding to the active state is a complex multi-step time-dependent process.

METHODS

Principles for measuring bimolecular fibrinogen binding to αIIbβ3 using laser tweezers

We used a model system to study individual ligand-receptor interactions that permits the measurement of discrete rupture forces produced by surface-bound ligand-receptor molecular pairs during repeated intermittent contact (Fig. 1 *A*). For these studies, purified αIIbβ3 was covalently bound to stationary pedestals anchored to the inside surface of a flow chamber (Fig. 1 *B*). Latex beads coated with fibrinogen were then flowed into the chamber. One of the latex beads was trapped by a laser and moved in an oscillatory manner so that the bead was intermittently in contact with a stationary pedestal. The tension produced when fibrinogen on the latex bead interacted with αIIbβ3 on the anchored pedestal caused a deflection of the laser beam that was sensed by a photodetector and displayed as a voltage signal that was proportional to the strength of ligand-receptor binding (Fig. 1 *C*). Rupture forces from interactions between several hundred pedestal-bead pairs were collected and displayed as normalized force distribution histograms for each experimental condition. To maximize single integrin-fibrinogen interactions while decreasing the likelihood of multiple interactions, the integrin and fibrinogen surface concentrations were deliberately decreased so that the fraction of contacts resulting in the formation of a specific bond between the receptor and the ligand with a yield force >10 pN was ~10% of bead-pedestal contacts or less. Accordingly, the majority of surface-to-surface touching events (≥90%) resulted in background noise or weak nonspecific interactions. The attachment of a fibrinogen-coated bead to an αIIbβ3-coated pedestal could be disrupted by a force of up to 200 pN applied by the trap.

Optical trap design and calibration

The core of our laser tweezers system is a Nikon (Melville, NY) Diaphot 300 inverted microscope and a 100× 1.3NA Fluor lens combined with a Spectra Physics (Mountain View, CA) FCBar Nd:YAG laser ($\lambda = 1064$ nm) with 4 W power in continuous TEM-00 mode (Fig. 2). A computer-operated two-dimensional acousto-optical deflector (Brimrose Corporation of America, Baltimore, MD) is used to control the tilt of the incoming laser beam at the back focal plane of the microscope objective, thereby altering the trap position. Displacement of a bead from the trap center, and consequently the force exerted by the trap on the displaced bead, are directly proportional to the beam deflection at the back focal plane of the condenser and are measured with a quadrant detector (30). The output currents from the four quadrants of the photodiodes are converted to voltages and the four voltages are combined to yield two voltages proportional to forces in the x and y directions (Fig. 2). These signals are filtered at 1 kHz and amplified (Series 902, Frequency Devices Amplifiers, Haverhill, MA) and then digitized at 2000 samples/s using a PC via an analog-to-digital converter board (catalogue No. PC-MIO-16E-4, National Instruments, Austin, TX). The voltage signal produced by the photodiode is calibrated in force units using the power spectrum of Brownian motion (31). Manipulations are recorded by a video CCD camera. All experiments are conducted at an average trap stiffness, $k = 0.22 \pm 0.01$ pN/nm (± SD), as computed from measurements of the bandwidth of Brownian motion for different beads using the equation: $k = f_c \times 2\pi\beta$, where k is the trap stiffness, f_c the corner frequency, and $\beta = 6\pi\eta r$ (η, viscosity; r, bead radius) (31). Force calibration and trap stiffness are routinely confirmed by the Stokes' force method (31). LabVIEW software (National Instruments) is used to control and record laser beam deflection, move the piezoelectric stage (Queensgate Instruments, Berkshire, UK), and for subsequent off-line data analysis.

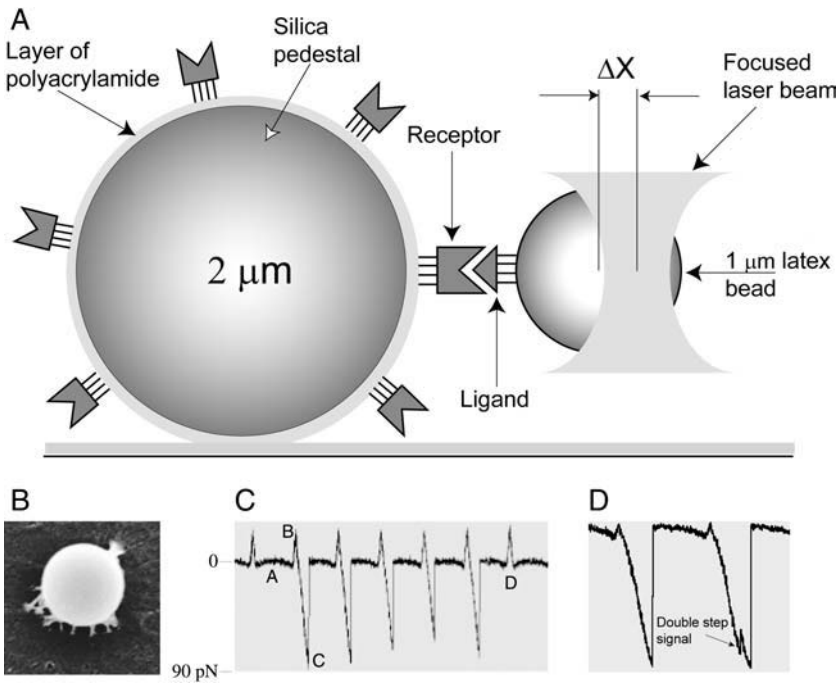

FIGURE 1 (*A*) Schematic drawing of the model system to study individual receptor-ligand interactions using laser tweezers. The latex bead coated with ligand molecules was trapped by the focused laser beam while moving toward or away from the silica pedestal coated with polyacrylamide gel-bound receptor molecules, touching it repeatedly. When the pedestal and the latex bead bound, the bead position remained nearly constant as the laser trap continued to move. The force on the bead increased proportionally to the displacement of the laser focus (ΔX) from the bead. (*B*) Scanning electron microscope image of a 2-μm silica bead anchored to the bottom of a chamber with polyacrylamide (*upper view*). (*C*) A portion of digitized data showing the force exerted by the trap on the latex bead during a series of contacts (positive upward deflections) and separations (negative downward deflections).(*Point A*) In the absence of contact between the bead and the pedestal the measured force was small. (*Point B*) At the moment of contact the laser trap exerted a positive, compressive force on the pedestal and the latex bead. The trap motion then reversed and the compressive force declined to zero. Peak *B* represents contact duration time between the surfaces. (*Point C*) When the integrin-fibrinogen pair binds, either specifically or nonspecifically, the force on the bead increased in the negative direction almost linearly until the pedestal-bead bond was ruptured and the force rapidly returned to nearly zero. (*Point D*) If no attachment occurred, there was no negative force. (*D*) An example of rare jagged signals reflecting stepwise unbinding in the case of multiple receptor-ligand interactions.

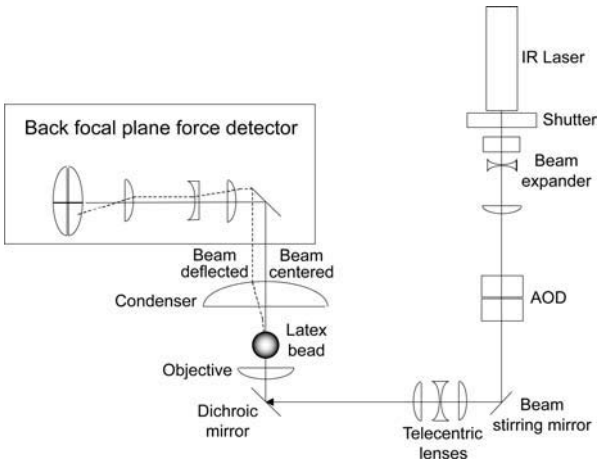

FIGURE 2 Optical scheme of the laser tweezers setup. The optical trap is generated with a 4-W Nd:YAG laser ($\lambda = 1064$ nm, Spectra Physics). A two-dimensional acousto-optical deflector (Brimrose Corporation of America) enables rapid ($\sim 3\ \mu$s) electronic control of the trap position. Bead forces are measured with a ''back focal plane'' force detector (71,72). The detectors are quadrant photodiodes (Current Designs, Philadelphia, PA) placed at a plane optically conjugate to the back focal plane of the condenser. The intensity distribution at the quadrant detectors indicates the deflection of the bead relative to the center of the trap, which is proportional to the applied force.

Preparation of αIIbβ3-coated pedestals and fibrinogen-coated beads

αIIbβ3-coated pedestals were prepared using silica microspheres 1.8–2.0 μm in diameter, as previously described (29). Briefly, a suspension of microspheres (5% v/v) in 30% (w/v) acrylamide/bis-acrylamide containing 2% (v/v) *N*,*N*,*N*′,*N*′-tetramethylethylenediamine and 2% (v/v) amyl acetate was uniformly spread on a clean, dry microscope glass coverslip and air-dried. Then, a freshly prepared saturated water solution of ammonium persulfate (2 μl) was smeared uniformly over the surface. A microscopic chamber (25–50 μl in volume) was assembled, with double-stick tape, from a glass slide and the polyacrylamide/pedestal-coated coverslip. After activation of the polyacrylamide-coated surface with glutaraldehyde (10% v/v, 4 h at room temperature) and thorough washing with the binding buffer (0.055 M borate buffer, pH 8.5), purified human αIIbβ3 (1 mg/ml) in the binding buffer with 150 mM NaCl and 1 mM $CaCl_2$ was immobilized for 12–16 h at 4°C. The integrity of αIIbβ3 heterodimers at alkaline pH and the lack of substantial oligomerization in the absence of octyl glucoside before immobilization were confirmed by transmission electron microscopy using rotary shadowing with tungsten (not shown). After washing to remove noncovalently adsorbed protein, 2 mg/ml bovine serum albumin (BSA) in 0.055 M borate buffer, pH 8.5, containing 1 mM $CaCl_2$ was added as a blocker. When Mn^{2+} was used to activate αIIbβ, the integrin was pretreated with 1 mM Mn^{2+} for 30 min at 37°C, and then it was immobilized in the storage buffer containing the same Mn^{2+} concentration. αIIbβ3 antagonists were added to the suspension of fibrinogen-coated beads before they were introduced into the chamber.

To confirm that the protocol described above resulted in covalent binding of protein to the polyacrylamide-coated beads, the protocol was used to attach fluorescein isothiocyanate-conjugated BSA (FITC-BSA) to the pedestal surface. FITC-BSA (1 mg/ml in binding buffer) was incubated as described in either a glutaraldehyde-activated chamber or a control untreated chamber. After thorough washing, the chambers were examined using a fluorescence microscope. The bottoms of both chambers, as well as the coated pedestals were highly fluorescent. The chambers were then washed successively with 20-fold volumes of 4 M urea/1 M NaCl/0.1% SDS and reexamined. The fluorescence of the glutaraldehyde-activated chamber did not change, whereas the adsorbed FITC-BSA was washed out of the control chamber. Further, many pedestals in the untreated chamber detached after treatment with the chaotropic agents, suggesting that glutaraldehyde, besides chemical activation of surfaces, cross-linked and anchored the pedestals to the polyacrylamide-coated coverslip as shown in Fig. 1 *B*.

For experiments measuring streptavidin binding to biotin, recombinant streptavidin (Sigma, St. Louis, MO) was adsorbed onto pedestals whose surface was covalently coated with biotin-BSA to spatially orient the streptavidin molecules. Biotin-coated latex microspheres 1 μm in diameter were purchased from Sigma. Preincubation of a streptavidin-containing chamber with free biotin almost completely abrogated bead attachment, confirming the specificity of the streptavidin-biotin binding measured by the laser tweezers.

Human fibrinogen was covalently bound to 0.93 μm carboxylate-modified latex beads (Bangs Laboratories, Fishers, IN) using *N*-(3-dimethylaminopropyl)-*N*′-ethylcarbodiimide hydrochloride as a cross-linking agent in a two-step procedure. After activation in 0.1 M 2-(*N*-morpholino)ethanesulphonic acid, pH 5.2, by mixing 1 ml of the buffer, 10 μl of a 10% bead suspension, 1.5 mg of dry carbodiimide, followed by constant shaking for 15 min at 4°C, the beads were sedimented, washed once with binding buffer (0.055 M borate buffer, pH 8.5), resedimented, and suspended in 20 μg/ml fibrinogen solution in binding buffer. After 15 min incubation with stirring at 4°C, the beads were sedimented and resuspended in BSA solution (2 mg/ml in 0.055 M borate buffer, pH 8.5) or 1 M ethanolamine solution in the same buffer. Fibrinogen-coated beads were freshly prepared and mildly sonicated to disrupt aggregates before each experiment.

The density of ^{125}I-fibrinogen on the surface of carbodiimide-activated beads depended on the concentration of fibrinogen in the binding solution (Fig. 3). The surface density of fibrinogen ranged from 2×10^{-9} to 11×10^{-9} μg/μm^2 or from 3.7×10^3 to 2.0×10^4 molecules/1 μm^2 (1×10^4–5.5×10^4 molecules/bead) with a saturation achieved at a fibrinogen concentration of $\sim$30 μg/ml.

αIIbβ3 heterodimers were isolated from detergent extracts of human platelets by affinity chromatography (32) and fibrinogen was purchased from American Diagnostica (Stamford, CT). The polypeptide composition, purity, and lack of oligomerization of αIIbβ3 and fibrinogen were assessed by SDS-polyacrylamide gel electrophoresis and by transmission electron microscopy using rotary shadowing with tungsten (33,34). Functionality of the αIIbβ3 preparations was confirmed by ability of the integrin to bind fibrinogen in solution and its susceptibility to activating effects of

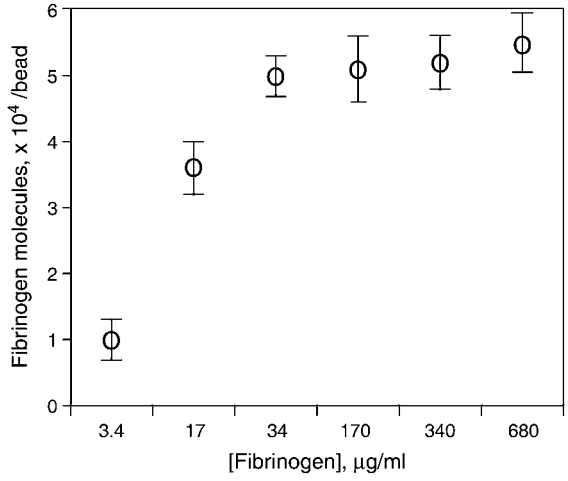

FIGURE 3 Number of fibrinogen molecules bound to each carbodiimide-activated carboxylate-modified bead as a function of initial fibrinogen concentration in the binding reaction mixture.

dithiothreitol and manganese ions (35). Fibrinogen was 95–97% clottable with thrombin, which confirms the high purity and activity of the protein.

Experimental procedure

To study the interaction between fibrinogen and purified αIIbβ3, 1 μl of a suspension of fibrinogen-coated beads (10^7 beads/ml) was added to 50 μl of 0.1 M HEPES buffer, pH 7.4, containing 2 mg/ml BSA, 0.1% Triton X-100, and 1 mM $CaCl_2$ (or $MnCl_2$). The mixture was introduced into a chamber containing αIIbβ3-coated pedestals. The experiments were performed in the presence of BSA and Triton X-100 to reduce the nonspecific interactions. After the chamber was placed on a microscope stage, a single bead was trapped by the laser beam. Using a manual stage, an αIIbβ3-coated pedestal was brought to within 1–2 μm of the trapped bead and the microscope focus was adjusted so that the bead and pedestal centers were the same distance from the coverslip surface (Fig. 1 *A*). The position of the laser trap was then oscillated in a triangular waveform with frequencies of 0.5 Hz, 5 Hz, or 50 Hz and a constant peak-to-peak amplitude of 800 nm. The distance separating the pedestal and the bead was reduced in 10-nm steps using the piezostage until repeated contacts were observed (Fig. 1 *C*). The piezostage position was adjusted so that the peak compressive force was 10–30 pN (Fig. 1 *C*, peak *B*) or the duration of contact was 2–5 ms at a 50-Hz oscillation frequency. When fibrinogen was bound to αIIbβ3, the bead stopped moving and a linear increase in force (loading rate) was observed (Fig. 1 *C*, peak *C*). If force ramps were not observed within 30 s, the bead was moved to a new pedestal surface. The integrin and fibrinogen surface concentrations were adjusted so that one in two pedestals produced detectable bonds. The loading rate depends on the trap stiffness and speed of separation of the pedestal and bead. Rupture forces were measured at the pulling speeds of 800, 8000, and 80,000 nm/s, corresponding to the three oscillation frequencies. With a 0.2-pN/nm trap stiffness, these are equivalent to loading rates of 160, 1600, and 16,000 pN/s, respectively. The loading rate for all experiments was 16,000 pN/s unless otherwise indicated. Data recording was initiated at first contact and was digitized at the rate of 2000 samples/s.

Data processing and analysis

The response time for the motion of a trapped bead that is not bound to a pedestal is <50 μs at the trap stiffness used. The bond ruptures were therefore observed as abrupt discrete decreases of trap force occurring within one sampling period (Fig. 1 *C*). The largest step decrease of force measured at times separated by two sample intervals during each period that the trap was moving away from the pedestal was counted as a rupture force. In the absence of bead-pedestal contacts and therefore of bond ruptures, the largest force transients were in the range of 0–10 pN and were due to Brownian noise. Data was recorded and analyzed with custom LabVIEW (National Instruments) programs.

The number of contacts recorded for each pedestal and bead pair depended on the oscillation frequency and was on average ~2000 contacts at 50 Hz, 850 contacts at 5 Hz, and 90 contacts at 0.5 Hz. For each bead pedestal pair the sequence of rupture forces were sorted into a histogram with 10-pN-wide bins and normalized by total number of contacts. The percentage of events in a particular force range (bin) represents the probability of a bond rupture in that force range. The first bin in the histograms, forces in the range of 0–10 pN, represented noise or optical artifacts in combination with weak nonspecific interactions. Accordingly, the first bin was neglected in data presentation and analysis. The results of experiments for multiple (~50) bead-pedestal pairs under similar conditions were averaged so that each probability histogram shown and/or analyzed in the Results section represented several thousand to $\sim 10^5$ contacts between similar reacting surfaces. Each point of a probability histogram was calculated as an average ± SD from individual files collected from separate pedestal-bead pairs.

RESULTS

Rupture force distribution of the specific αIIbβ3-fibrinogen binding versus nonspecific protein-protein interactions

The distribution of rupture forces between αIIbβ3- and fibrinogen-coated surfaces ranged from several piconewtons to 150 pN, with the probability of forces >130 pN being <0.01% (Fig. 4, curve *1*). A typical histogram of yield forces omitting the 0–10 pN point contained two regimes of moderate and strong binding, corresponding to ~20–60 pN and 60–130 pN, respectively (Fig. 4).

The two components of the yield force histogram were then modeled with an empirically determined function as the sum of an exponential and a Gaussian curve, as described by Eq. 1:

$$Y = a_1 \times \exp(-x/b_1) + a_2 \times \exp(-((x-c)/b_2)^2). \quad (1)$$

This two-component fit was used to quantify the force distributions and to compare αIIbβ3-fibrinogen interactions registered under different experimental conditions (see Tables 2–4). The rupture forces in the range 20–60 pN were typically well fit with an exponential and stronger yield forces in the range 60–130 pN were well fit with a Gaussian curve centered at ~80–90 pN. The fit parameter b_1 gives the

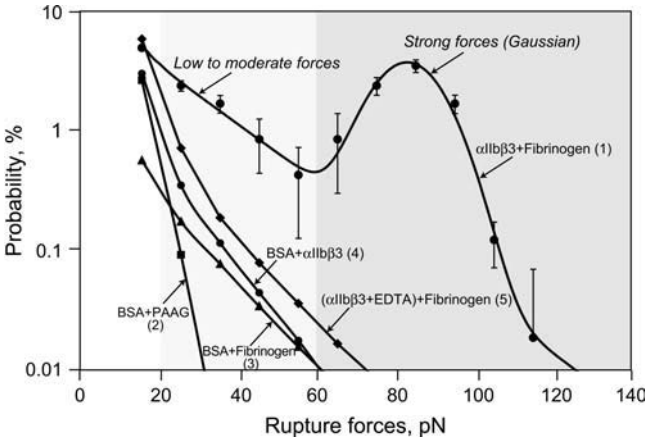

FIGURE 4 Yield force distribution of forces required to rupture interactions between integrin αIIbβ3- and fibrinogen-coated beads (curve *1*) compared to nonspecific interactions (curves *2–5*). The rupture force distribution of the integrin-fibrinogen interactions is fitted with a sum of an exponential and a Gaussian function. The number of ruptures >10 pN used to plot curve *1* is 19,788 (19.8% of the total number of contacts, $n = 99{,}938$). The zero point (0–10 pN bin), which represented the remaining 80.2%, is omitted. The different force regimes are marked with the backgrounds of various intensities. The probability of moderate or strong force interactions is higher for integrin-fibrinogen than for nonspecifically interacting protein-coated surfaces: (curve *2*) BSA-coated beads with untreated polyacrylamide-coated pedestals (2.8% ruptures >10 pN, $n = 9{,}988$); (curve *3*) fibrinogen-coated beads with BSA-coated pedestals (0.9%, $n = 16{,}885$); (curve *4*) BSA-coated beads with integrin αIIbβ3-coated pedestals (3.6%, $n = 35{,}334$); and (curve *5*) fibrinogen-coated beads with EDTA-pretreated integrin αIIbβ3 bound to pedestals (7.6%, $n = 14{,}134$). The points in curve *1* represent averages from individual pedestal-bead pairs ± SD.

average and c gives the most probable rupture forces for the moderate and strong interactions, respectively.

To distinguish between specific and nonspecific binding (36), two types of control experiments were performed. In the first type, one or both ligand and receptor molecules were omitted or substituted with noninteracting proteins (Fig. 4, curves *2–5*). In the second, inhibitors specific to αIIbβ3 were used to reduce or eliminate specific interactions (Table 1). The majority of rupture forces were <20 pN for all the surface treatments (Fig. 4) and inhibitors (Table 1). For the αIIbβ3-fibrinogen interactions, ruptures >20 pN accounted for ~15% of the interactions whereas for the control surfaces the probability for observing ruptures >20 pN was in the range 0.08–1.0% (Fig. 4). The weakest interactions, with all ruptures occurring at forces <30 pN, were observed for untreated polyacrylamide-coated pedestals in contact with BSA-coated beads (Fig. 4, curve *2*). Pedestal surfaces were slightly more reactive with BSA-coupled beads after covalent coupling with fibrinogen (Fig. 4, curve *3*) or with intact αIIbβ3 (Fig. 4, curve *4*). The most effective inhibitor was pretreatment of the αIIbβ3 with EDTA (1 mM) before and during the immobilization of αIIbβ3 to the pedestals. EDTA causes dissociation of αIIbβ3 into its two subunits, thereby destroying specific fibrinogen-binding sites (34,37). The probability for rupture forces >20 pN during the interaction of EDTA-treated αIIbβ3 molecules with fibrinogen was higher than any of the surface controls but still >15-fold lower than for intact αIIbβ3- and fibrinogen-coated surfaces (Fig. 4, curve *5*). These data suggest that nearly all of the nonspecific interactions are limited to ruptures (at 16,000 pN/s loading rate) occurring at <20 pN, >90% of the ruptures in the range 20–60 pN are likely specific interactions, and virtually all of the ruptures occurring at >60 pN are specific. Accordingly, the remaining analysis will focus exclusively on ruptures at forces >20 pN.

TABLE 1 Effect of specific αIIbβ3 antagonists on the distribution of αIIbβ3-fibrinogen rupture forces within different force regimes

Inhibitors	Force regimes				Total number of contacts
	20–60 pN		>60 pN		
H12-peptide (1 mM)	123	0.6%	348	1.7%	20,486
Without the inhibitor	506	2.9%	940	5.4%	17,439
Tirofiban (50 μM)	113	0.4%	308	1.2%	25,741
Without the inhibitor	468	2.1%	763	3.4%	22,290
RGDS peptide (1 mM)	155	0.8%	308	1.5%	20,037
Without the inhibitor	524	2.8%	703	3.8%	18,297
mAb A2A9 (100 μg/ml)	148	0.9%	108	0.6%	17,074
Without the inhibitor	333	2.2%	511	3.3%	15,336
abciximab (100 μg/ml)	268	1.0%	174	0.7%	25,371
Without the inhibitor	377	1.9%	497	2.4%	20,298
Noninhibitory mAb SSA6 (100 μg/ml)	160	1.2%	203	1.5%	13,412
Without mAb SSA6	298	1.6%	368	1.9%	18,937

Values in Table 1 are presented as number of events and percentage of total number of contacts.

Discriminating single versus multiple αIIbβ3-fibrinogen bonds

Several criteria were used to test whether the observed ruptures were due to single or multiple bonds (29,38). First, the rupture of interactions due to multiple bonds should occur in a sequence of multiple steps, whereas the rupture due to single bonds should always occur in a single step. Typically 99.8–99.9% of the ruptures occurred in one step (as in Fig. 1 *C*) and 0.1–0.2% occurred in two or more steps separated by >0.5 ms (as in Fig. 1 *D*). The bond ruptures that occurred in multiple steps were not included in the histograms.

Second, the histograms of the distribution of rupture forces of multiple identical interactions should appear as a series of quantized peaks that are multiples of a single value of force and have probabilities inversely proportional to the number of bonds. For the strong interactions we observed only a single well-defined peak in the force histograms (Fig. 4, curve *1*).

Third, the yield strength for single bonds should be independent of the surface density of either the receptor or ligand (39). The surface density of fibrinogen molecules was changed over the range 3.7×10^3–2.0×10^4 molecules/1 μm^2 by changing its initial concentration from 3.4 to 640 μg/ml in the binding solution added to the activated latex beads (Fig. 3). The highest value is comparable with the saturating surface density of fibrinogen reported by others (40). Rupture forces between surface-bound fibrinogen and αIIbβ3 molecules were measured using beads prepared under identical conditions with three substantially different fibrinogen surface densities. To control for the variability of the integrin preparation, the three bead preparations synthesized were flowed, in succession, through a chamber containing αIIbβ3-coated pedestals and rupture force distributions were measured (Table 2). The rupture forces for both the moderate and strong force ranges remained unchanged. The average cumulative probability for binding events with rupture forces >20 pN varied from 0.6% to 2.7% (Table 2) and the probabilities depended linearly on fibrinogen surface density for both the moderate and the strong interaction regimes of the yield forces (Fig. 5). Thus, variations in surface density of fibrinogen correlate directly with changes in the probability of fibrinogen-integrin binding but they have no effect on the yield strength.

TABLE 2 Yield strength and probability of the αIIbβ3-fibrinogen interactions with different fibrinogen surface density

Fibrinogen surface density, $\mu g/\mu m^2$	Yield strength, pN		Cumulative probability (%)	
	20–60 pN	>60 pN	20–60 pN	>60 pN
2×10^{-9}	32.6 ± 1.1	79.1 ± 1.5	0.32 ± 0.09	0.19 ± 0.04
7×10^{-9}	30.6 ± 1.6	76.4 ± 1.8	0.86 ± 0.16*	0.57 ± 0.08†
11×10^{-9}	32.8 ± 1.4	76.9 ± 1.2	1.59 ± 0.35*	1.04 ± 0.27†

*,† $p < 0.01$.

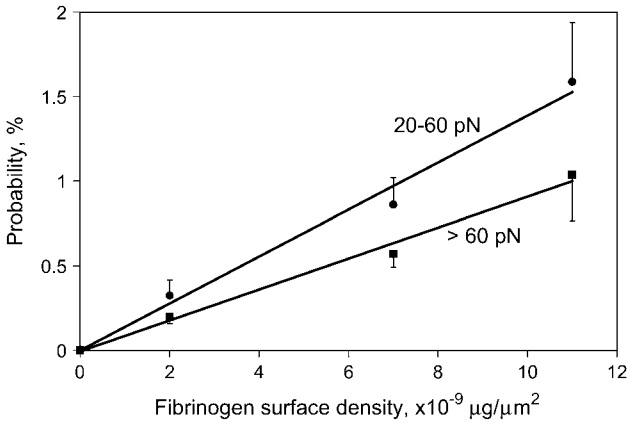

FIGURE 5 The probability of observing moderate (20–60 pN) and strong (>60 pN) binding forces between integrin αIIbβ3 and fibrinogen as functions of the fibrinogen surface density. The number of ruptures >20 pN included in the analysis were 258 (0.6%; number of contacts, $n = 42{,}998$) for fibrinogen surface density of 2×10^{-9} μg/μm^2, 541 (1.5%, $n = 36{,}072$) for 7×10^{-9} μg/μm^2, and 862 (2.7%, $n = 31{,}921$) for 11×10^{-9} μg/μm^2. The results are shown as an average from individual pedestal-bead pairs ± SD.

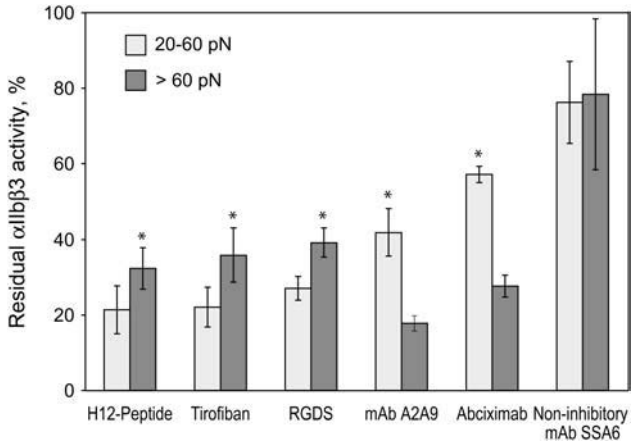

FIGURE 6 Effect of integrin αIIbβ3 antagonists on αIIbβ3-fibrinogen binding. The relative probability for forming bonds with rupture forces in the weaker (20–60 pN) and stronger (>60 pN) rupture force regimes for integrin αIIbβ3 treated with 1 mM H12-peptide (fibrinogen-binding inhibitor dodecapeptide) ($n = 30{,}473$), 40 μM tirofiban ($n = 61{,}056$), 1 mM RGDS ($n = 88{,}178$), 100 μg/ml αIIbβ3-binding specific ''antiaggregant'' monoclonal antibodies A2A9 ($n = 46{,}353$), 100 μg/ml abciximab ($n = 32{,}469$), and 100 μg/ml noninhibitory αIIbβ3-specific mAb SSA6 ($n = 13{,}412$) normalized to untreated αIIbβ3 ($^*p < 10^{-3}$ for comparative inhibitory efficacy in the lower and higher force regimes). Positive control data with untreated αIIbβ3 were collected for each of the inhibitors in the same chamber before addition of an inhibitor and were statistically comparable by the number of contacts (Table 2). The results are shown as an average from individual pedestal-bead pairs ± SD.

These data suggest that the surface density of receptor and ligand are low enough so that at most one integrin-fibrinogen bond is formed during each contact.

The moderate and strong force regimes respond differently to inhibition and enhancement of the αIIbβ3-fibrinogen interactions

Our previous qualitative comparisons of yield force distributions between fibrinogen and αIIbβ3 suggested that the moderate and strong rupture forces resulted from specific fibrinogen binding to αIIbβ3, whereas the weak forces were nonspecific (29). However, further study of the moderate and strong yield force regimes have revealed a number of differences in addition to the magnitude of the rupture force required to disrupt fibrinogen binding to αIIbβ3. First, small-molecule αIIbβ3 antagonists such as the fibrinogen γ chain peptide H12 peptide, the peptidomimetic tirofiban, and the tetrapeptide Arg-Gly-Asp-Ser (RGDS) were most effective in inhibiting moderate force interactions, whereas the inhibitory monoclonal antibodies A2A9 and abciximab were substantially more effective in inhibiting strong interactions (Fig. 6). Second, whereas preincubation of the fibrinogen-coated latex beads with soluble αIIbβ3 molecule abrogated stronger αIIbβ3-fibrinogen interactions, they augmented rupture forces in the moderate range, perhaps as a consequence of αIIbβ3-αIIbβ3 binding (1) (not shown). Third, the relative probability of detecting moderate and strong rupture forces was affected by the length of time the αIIbβ3 preparation had been stored at 4°C (Fig. 7). We found that the most labile component of the αIIbβ3-fibrinogen interaction was the strong force regime, which decreased as a function of the time of storage, whereas there was no corresponding change in the moderate force regime. Fourth, we found that Mn^{2+}, a divalent cation which induces a conformational change in the extracellular domain αIIbβ3 that increases its affinity for fibrinogen (35), enhanced the strong component of the yield force distribution >2.5-fold, but increased the moderate component only 1.5-fold ($p < 0.01$) (Fig. 8). However, the αIIbβ3 antagonists, tirofiban and abciximab, both effectively abrogated both types of binding

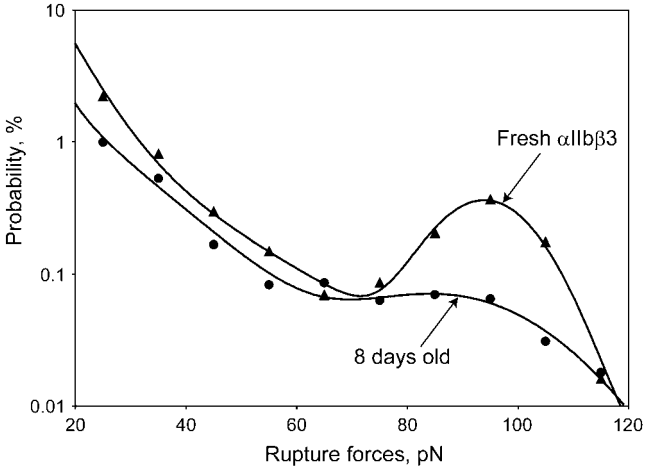

FIGURE 7 Effect of storage of the integrin αIIbβ3 preparation at 4°C on the yield force distribution of the integrin αIIbβ3-fibrinogen interactions (data from an individual experiment with 31,936 contacts for fresh integrin and 37,174 for the same integrin preparation after 8 days of storage).

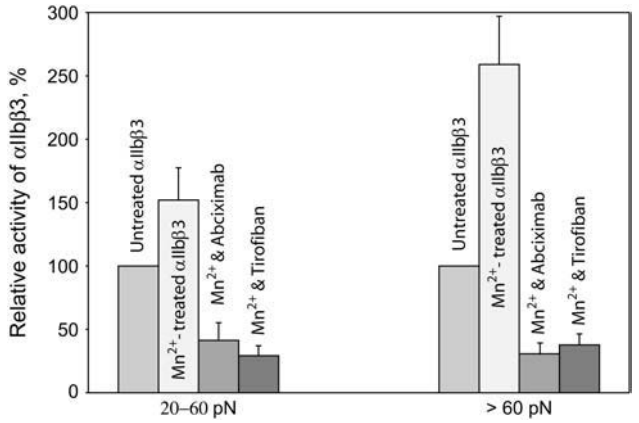

FIGURE 8 Effect of Mn^{2+} on the fibrinogen binding activity of integrin αIIbβ3 in the absence and presence of 50 μM tirofiban and 100 μg/ml abciximab in the lower (20–60 pN) and higher (>60 pN) yield force regimes. The data were collected at 5-Hz bead oscillation frequency using 12–50 different pedestal-bead pairs for each experimental condition. There were 1,663 ruptures >20 pN used to plot the bar graphs for control αIIbβ3-fibrinogen interactions without Mn^{2+} (5.9% of total contacts, $n = 28,203$) and 4,587 ruptures (10% of contacts, $n = 45,871$) used to plot bar graphs for interactions with Mn^{2+}. In the presence of Mn^{2+} and tirofiban the number of >20-pN ruptures was 201 (0.94%, $n = 21,383$); in the presence of Mn^{2+} and abciximab they were 164 (1.7%, $n = 9,647$). Each point is calculated as an average from individual pedestal-bead pairs ± SD.

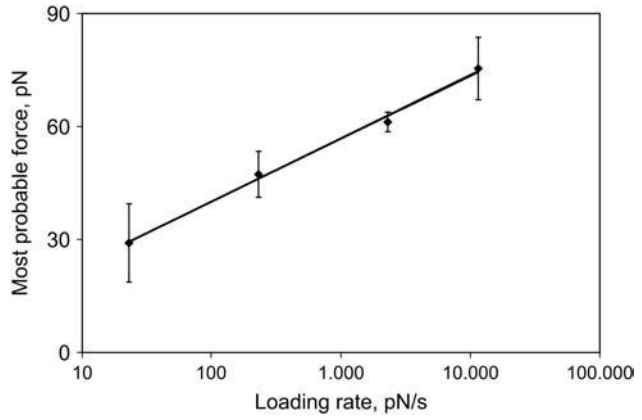

FIGURE 9 Dependence of the yield strength of streptavidin-biotin interactions on the loading rate. The number of forces >20 pN included in the analysis were 74 (14%, $n = 528$) for the loading rate of 23 pN/s (0.1-Hz bead oscillation frequency), 82 (4%, $n = 2,057$) for 230 pN/s (1 Hz), 792 (6%, $n = 13,196$) for 2,300 pN/s (10 Hz), and 1,091 (5%, $n = 21,825$) for 11,500 pN/s (50 Hz). Each point is calculated as an average from individual pedestal-bead pairs ± SD.

forces in the presence and absence of Mn^{2+} suggesting that they represent specific αIIbβ3-fibrinogen binding and unbinding.

Dependence of the yield force on loading rates and contact duration

Changes in the yield force distribution with loading rate can be used to estimate the energy landscape and kinetic parameters for a particular receptor-ligand pair (41–45). To change both the loading rate and contact duration in our experiments, we varied the oscillation frequency.

Since the loading rate dependence of rupture forces was first demonstrated for streptavidin-biotin interactions (45), we used this receptor-ligand pair to validate our experimental protocol and subsequent analysis. The effect of loading rate on the rupture force distributions for biotin-streptavidin interactions is shown in Fig. 9. The most probable rupture force (yield strength) of the strong force distribution was linearly dependent on the log of the loading rate and increased 2.5-fold when the loading rate changed from 23 to 11,500 pN/s. The transition state distance or location of the activation barrier calculated from the slope (42) was found to be ~0.5 nm, in good agreement with previous data obtained using a biomembrane force probe (45). Increasing the loading rate to 23,000 pN/s resulted in a further shift of the rupture forces such that the laser trap was most often unable to separate bound molecules.

Similar experiments examining fibrinogen binding to αIIbβ3 produced very different results (Fig. 10). The yield strength for the strong force component of fibrinogen binding to αIIbβ3 was independent of loading rates in the range of 160–16,000 pN/s (Table 3). On the other hand, the cumulative probability of strong fibrinogen-αIIbβ3 interactions was inversely proportional to the oscillation frequency and directly proportional to the duration of contact, reaching almost 9% at the lowest loading rate and the greatest contact duration studied. Surprisingly, the average rupture force for the moderate force regime decreased at higher oscillation frequencies. As expected, the cumulative probability for the moderate force component decreased at higher oscillation frequencies and increased with increasing contact duration (Table 4).

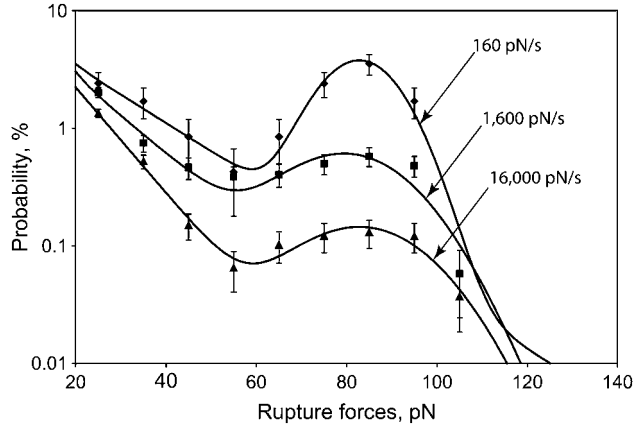

FIGURE 10 Rupture force distribution of the integrin αIIbβ3-fibrinogen interactions at different loading rates. The data were collected during repeated touching of the same surfaces (19 pedestal-bead pairs) at different bead oscillation frequency. The total number of contacts included in the histograms was 1,784 for 160 pN/s (0.5 Hz), 13,311 for 1,600 pN/s (5 Hz), and 51,535 for 16,000 pN/s (50 Hz). Each point is calculated as an average from individual pedestal-bead pairs ± SD.

TABLE 3 Yield strength and cumulative probability of the strong (>60 pN) αIIbβ3-fibrinogen interactions at different loading rates and contact duration

Loading rate (pN/s)	Contact duration (s)	Yield strength (pN)	Cumulative probability (%)
160	0.320 ± 0.118	82.9 ± 1.5	8.6 ± 2.5
1,600	0.030 ± 0.009	80.1 ± 2.1	1.9 ± 0.5
16,000	0.004 ± 0.001	83.2 ± 2.9	0.5 ± 0.2

TABLE 4 Yield strength and cumulative probability of the moderate (20–60 pN) αIIbβ3-fibrinogen interactions at different loading rates and contact duration

Loading rate (pN/s)	Contact duration (s)	Yield strength (pN)	Cumulative probability (%)
160	0.320 ± 0.118	43.1 ± 4.6	2.00 ± 0.42
1,600	0.030 ± 0.009	35.6 ± 3.2	0.58 ± 0.18
16,000	0.004 ± 0.001	31.5 ± 2.1	0.27 ± 0.07

Because there was variation in contact duration at the same oscillation frequency, the interaction probabilities versus contact duration were analyzed in more detail. We found that the dependence of interaction probability on contact duration differed for each component of the rupture force histogram (Fig. 11). Thus, the probability of detecting weaker binding interactions is greater than for stronger interactions during brief contacts, suggesting that the weaker interactions form faster.

DISCUSSION

Using laser tweezers-based force spectroscopy, we studied the rupture force profile of bimolecular αIIbβ3-fibrinogen interactions, which appeared as a complex bimodal force distribution with at least two regimes, namely 20–60 pN and >60 pN. The rupture force regimes turned out to be substantially different in a number of important characteristics, implying that they reflected interactions of different origin.

Based on several criteria that have been proposed to test whether the observed ruptures were due to single or multiple bonds (29,38), our data strongly indicate that under the experimental conditions studied the rupture events were due to single bonds. First, the rupture of bonds occurred in a single step in >99% of force counts. Second, the histograms of the distribution of rupture forces did not appear as a series of peaks, as would be predicted if the identical interactions were multiple. Third, the binding strength was constant at increased surface densities of the interacting proteins, showing that only one αIIbβ3-fibrinogen pair was involved irrespective of the number of molecules present on the surfaces (Table 2). Fourth, the probability of both moderate and strong interactions increased linearly with the density of molecules on the surfaces (Fig. 5), consistent with single-molecule binding.

To ensure that the majority of the rupture events were due to single bonds, the experimental conditions were tuned to keep the frequency of binding between αIIbβ3-coated pedestals and fibrinogen-coated beads low, specifically so that only 1–10% of total interface contacts resulted in interactions with ruptures >20 pN. To accumulate a statistically significant number of events and compensate for these low probabilities, a very large number of contacts was required. The ability to collect data with large numbers of contacts is one of the main advantages of the rupture force assay based on an oscillating optical trap.

The force limit of our measurement system, as determined by thermal fluctuations of the trapped bead, is ~10 pN. Therefore, only those bonds that rupture at forces in the range 10–200 pN are detectable. Careful control experiments (Fig. 4, curves *2–5*) show that the large majority of the nonspecific interactions occur with rupture forces <20 pN. Accordingly, we focused our attention on the yield forces in the range 20–200 pN, which was segregated into moderate (20–60 pN) and strong (>60 pN) force regimes. The moderate and strong rupture force regimes both resulted from fibrinogen bound to αIIbβ3, but were different in a number of important characteristics. The kinetic behavior for the two force regimes was different, with the weaker interactions forming faster than the stronger ones, suggesting a complex pathway for αIIbβ3 and fibrinogen interactions that could result from either multiple receptor-ligand binding/unbinding steps or from intermediate integrin receptor activation states. Consistent with the former possibility, we found that the moderate force interactions were more effectively inhibited by small-molecule antagonists, whereas the strong interactions were more effectively inhibited by substantially larger anti-αIIbβ3 monoclonal antibodies. Moreover, the stronger forces were more labile during storage and were more sensitive to the perturbing effect of Mn^{2+} on the

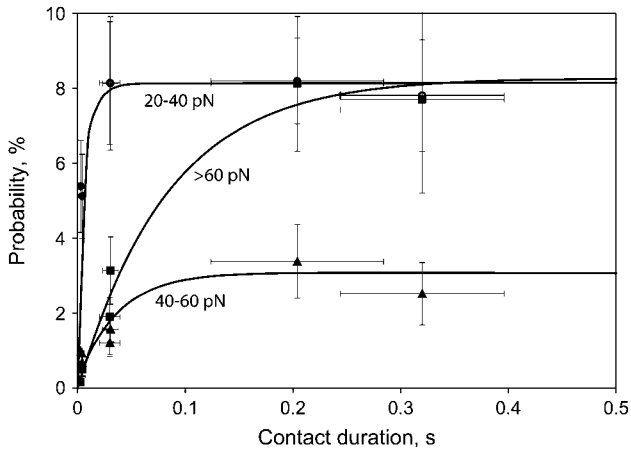

FIGURE 11 Probability for observing low (20–40 pN), moderate (40–60 pN), and strong (>60 pN) binding forces between integrin αIIbβ3 and fibrinogen depends on duration of contact between bead and pedestal. The contact time needed to reach half-maximal fibrinogen binding at a constant loading rate of 1,600 pN/s was ≈1 ms for the 20–40 pN, 20 ms for the 40–60 pN, and 70 ms for the >60 pN force regimes. Errors of cumulative probability (*Y*-scale) and contact duration (*X*-scale) were calculated as standard deviations.

conformation of the αIIbβ3 extracellular domain (35). Taken together, these data suggest a model for fibrinogen binding to αIIbβ3 in which their initial interaction is followed by reorganization of the binding interface, thereby enhancing the strength of binding (Fig. 12).

Consistent with this, it has been reported that purified αIIbβ3 binds to fibrinogen in a time-dependent two-step process. Thus, after rapidly reaching an initial reversible bound state, the αIIbβ3-fibrinogen complex becomes more stable (8) and dissociates only in the presence of high concentrations of the tetrapeptide Arg-Gly-Asp-Val, or RGDV (7). Time dependence is also observed when a load is imposed on the interaction. For example, Goldsmith et al. (6) found that the shear-induced breakup of αIIbβ3-coated latex spheres cross-linked by fibrinogen depended on the time of contact between the spheres, suggesting the existence of ''young'' weak versus ''old'' strong αIIbβ3-fibrinogen interactions.

An alternative explanation for our data, illustrated in Fig. 13, is based on the assumption that αIIbβ3 exists in a number of activation states having different ligand-binding affinities. This alternative posits that the various ligand-binding affinities depend on the nature and/or amount of integrin-activating stimuli (46–52). Although our data are not, by themselves, sufficient to differentiate between these models, there are a number of arguments that favor ''multiple binding steps'' over ''multiple activation states''. First, structural studies of αIIbβ3 and another integrins performed using transmission electron microscopy and x-ray crystallography revealed either open or closed molecular conformations without intermediate forms (35,53). Second, platelet stimulation, using ADP or the thrombin receptor activating peptide, TRAP, enhances the accessibility, but not the adhesion strength of single αIIbβ3 molecules, consistent with the presence of only two αIIbβ3 activation states (29). Third, analysis of rupture force spectra obtained for αIIbβ3 and fibrinogen in ADP-stimulated platelets (29) did not reveal changes in the moderate force regime as the ADP concentration increased, indicating that fibrinogen-binding affinity of individual αIIbβ3 molecules is either on or off, regardless of the strength of the platelet stimulus.

It should be mentioned that the moderate force regime might reflect partially denatured protein molecules rather than an intermediate receptor binding step or activation state. The data presented in this work are not, by themselves, sufficient to exclude this artifact; however, the moderate force regime was observed not only with purified proteins

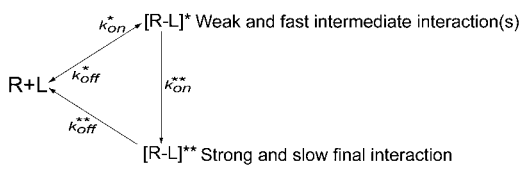

FIGURE 12 Schematic presentation of multiple receptor-ligand binding/unbinding steps.

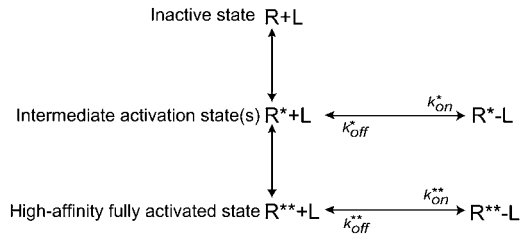

FIGURE 13 Schematic presentation of multiple receptor activation states.

but also in live platelets where the integrin is secured from denaturing (29,38). As to fibrinogen, its functional homogeneity on the surface of latex beads was demonstrated in binding experiments with fibrin and its fragments (R. Litvinov, O. Gorkun, S. Owen, H. Shuman, and J. Weisel, unpublished data), with uniform and strong rupture forces showing up as one sharp peak without any intermediate force regime.

Dynamic force spectroscopy has been used to extract the thermodynamic and kinetic characteristics of specific intermolecular interactions underlying receptor-ligand binding. In most cases, the average rupture force, or yield strength, increased with loading rate and displayed mono- or multiphasic logarithmic dependence over a wide range of loading rates (17,19,54–59). However, the loading rate dependence for αIIbβ3-fibrinogen unbinding did not follow this trend. The yield strength for the strong force regime was ~82 pN, independent of loading rates >3 orders of magnitude. The constant yield strength likely reflects intrinsic properties of αIIbβ3 because control experiments with biotin-streptavidin reproduced earlier measurements using other techniques (45). A constant yield strength implies that the transition state distance is large (43) and has been observed for several other receptor-ligand pairs (60–62). The yield strength for the moderate force regime (Fig. 10, Table 2) decreased at higher loading rates. Although an inverse relationship between rupture force and loading rate is counterintuitive, it has also been observed in other systems (63,64) and may reflect a failure of the simplest model for unbinding (65–68).

It was noted earlier that the probability of integrin-fibrinogen binding changes inversely with oscillation frequency and is attributable to changes in contact duration, as was demonstrated earlier for the interactions between fibronectin and bacterial adhesion molecules (69). Accordingly, the decreasing yield strength of the moderate force interactions may be due to changes in contact duration between the bead and pedestal at different oscillation frequencies. For example, as shown in Fig. 11, the moderate interactions (20–60 pN) may have two components: rapid interactions at 20–40 pN and slower interactions at 40–60 pN so that at high oscillation frequency (short contact duration), the lowest force interactions predominate. However, because loading rate and contact duration change with oscillation frequency, it is not at present possible to discriminate between these two possibilities.

In conclusion, our data suggest that fibrinogen binding to αIIbβ3 is a complex, time-dependent, multi-step process, during which the strength of the bond between αIIbβ3 and fibrinogen appears to progressively increase. This may be of physiological importance because fibrinogen binding to αIIbβ3 occurs in an environment where contact duration is determined by shear. Moreover, it may account for von Willebrand factor-mediated slowing of platelet velocity required to establish a stable αIIbβ3-mediated platelet thrombus (70).

This work was supported by grants HL57407, HL30954, HL40387, and HL62250 from the National Institutes of Health.

REFERENCES

1. Li, R., N. Mitra, H. Gratkowski, G. Vilaire, R. Litvinov, C. Nagasami, J. W. Weisel, J. D. Lear, W. F. DeGrado, and J. S. Bennett. 2003. Activation of integrin αIIbβ3 by modulation of transmembrane helix associations. *Science*. 300:795–798.
2. Shattil, S. J., H. Kashiwagi, and N. Pampori. 1998. Integrin signalling:the platelet paradigm. *Blood*. 91:2645–2657.
3. Kim, M., C. V. Carman, and T. A. Springer. 2003. Bidirectional transmembrane signaling by cytoplasmic domain separation in integrins. *Science*. 301:1720–1725.
4. Bennett, J. S. 1996. Structural biology of glycoprotein IIb-IIIa. *Trends Cardiovasc. Med.* 16:31–36.
5. Hu, D. D., C. A. White, S. Panzer-Knodle, J. D. Page, N. Nicholson, and J. W. Smith. 1999. A new model of dual interacting ligand binding sites on integrin αIIbβ3. *J. Biol. Chem.* 274:4633–4639.
6. Goldsmith, H. L., F. A. McIntosh, J. Shahin, and M. M. Frojmovic. 2000. Time and force dependence of the rupture of glycoprotein IIb-IIIa-fibrinogen bonds between latex spheres. *Biophys. J.* 78:1195–1206.
7. Huber, W., J. Hurst, D. Schlatter, R. Barner, J. Hubscher, W. C. Kouns, and B. Steiner. 1995. Determination of kinetic constants for the interaction between the platelet glycoprotein IIb-IIIa and fibrinogen by means of surface plasmon resonance. *Eur. J. Biochem.* 227:647–656.
8. Muller, B., H. G. Zerwes, K. Tangemann, J. Peter, and J. Engel. 1993. Two-step binding mechanism of fibrinogen to αIIbβ3 integrin reconstituted into planar lipid bilayers. *J. Biol. Chem.* 268:6800–6808.
9. Weisel, J. W., H. Shuman, and R. I. Litvinov. 2003. Protein-protein unbinding induced by force: single-molecule studies. *Curr. Opin. Struct. Biol.* 13:227–235.
10. Florin, E.-L., V. T. Moy, and H. E. Gaub. 1994. Adhesion forces between individual ligand-receptor pairs. *Science*. 264:415–417.
11. Helm, C., W. Knoll, and J. N. Israelashvili. 1991. Measurment of ligand-receptor interactions. *Proc. Natl. Acad. Sci. USA*. 88:8169–8173.
12. Israelashvili, J. N., D. E. Leckband, F. J. Schmitt, J. Zasadzinski, S. Walker, and S. Chirovolu. 1994. Direct measurement of specific ligand-receptor interactions between model membrane surfaces. *In* Studying Cell Adhesion. P. Bongrand, P. Claesson, and A. Curtis, editors. Springer, Heidelberg. 37–49.
13. Leckband, D. E., J. N. Israelashvili, F. J. Schmitt, and W. Knoll. 1992. Long range attraction and molecular rearrangements in receptor-ligand interactions. *Science*. 255:1419–1421.
14. Evans, E., D. Berck, and A. Leung. 1991. Detachment of agglutinin-bonded red blood cells. I-Forces to rupture molecular point attachments. *Biophys. J.* 59:838–848.
15. Tha, S. P., J. Shuster, and H. L. Goldsmith. 1986. Interaction forces between red cells agglutinated by antibody. II. Measurement of hydrodynamic force of breakup. *Biophys. J.* 50:1117–1126.
16. Lee, I., and R. E. Marchant. 2001. Force measurements on the molecular interactions between ligand (RGD) and human platelet $\alpha_{IIb}\beta_3$ receptor system. *Surf. Sci.* 491:433–443.
17. Lee, I., and R. E. Marchant. 2003. Molecular interaction studies of hemostasis: fibrinogen ligand-human platelet receptor interactions. *Ultramicroscopy*. 97:341–352.
18. Lehenkari, P. P., and M. A. Horton. 1999. Single integrin molecule adhesion forces in intact cells measured by atomic force microscopy. *Biochem. Biophys. Res. Commun.* 259:645–650.
19. Li, F., S. D. Redick, H. P. Ericksen, and V. T. Moy. 2003. Force measurements of the $\alpha_5\beta_1$ integrin-fibronectin interaction. *Biophys. J.* 84:1–11.
20. Ashkin, A. 1997. Optical trapping and manipulation of neutral particles using lasers. *Proc. Natl. Acad. Sci. USA*. 94:4852–4860.
21. Reichle, C., K. Sparbier, T. Muller, T. Schnelle, P. Walden, and G. Fuhr. 2001. Combined laser tweezers and dielectric field cage for the analysis of receptor-ligand interactions on single cells. *Electrophoresis*. 22:272–282.
22. Brouhard, G. J., H. T. Schek 3rd, and A. J. Hunt. 2003. Advanced optical tweezers for the study of cellular and molecular biomechanics. *IEEE Trans. Biomed. Eng.* 50:121–125.
23. Simmons, R. M., J. T. Finer, S. Chu, and J. A. Spudich. 1996. Quantitative measurements of force and displacement using an optical trap. *Biophys. J.* 70:1813–1822.
24. Nishizaka, T., H. Miyata, H. Yoshikawa, S. Ishiwata, and K. Kinosita Jr. 1995. Unbinding force of a single motor molecule of muscle measured using optical tweezers. *Nature*. 377:251–254.
25. Nishizaka, T., R. Seo, H. Tadakuma, K. Kinosita Jr., and S. Ishiwata. 2000. Characterization of single actomyosin rigor bonds: load dependence of lifetime and mechanical properties. *Biophys. J.* 79: 962–974.
26. Miyata, H., R. Yasuda, and K. Kinozita Jr. 1996. Strength and lifetime of the bond between actin and skeletal muscle α-actinin studied with an optical trapping technique. *Biochim. Biophys. Acta*. 1290:83–88.
27. Stout, A. L. 2001. Detection and characterization of individual intermolecular bonds using optical tweezers. *Biophys. J.* 80:2976–2986.
28. Rinko, L. J., M. B. Lawrence, and W. H. Guilford. 2004. The molecular mechanics of P- and L-selectin lectin domains binding to PSGL-1. *Biophys. J.* 86:544–554.
29. Litvinov, R. I., H. Shuman, J. S. Bennett, and J. W. Weisel. 2002. Binding strength and activation state of single fibrinogen-integrin pairs on living cells. *Proc. Natl. Acad. Sci. USA*. 99:7426–7431.
30. Visscher, K., and S. M. Block. 1998. Versatile optical traps with feedback control. *Methods Enzymol.* 298:460–489.
31. Visscher, K., S. P. Gross, and S. M. Block. 1996. Construction of multiple-beam optical traps with nanometer-resolution position sensing. *IEEE J. Sel. Top. Quantum Electron.* 2:1066–1076.
32. Bennett, J. S., J. A. Hoxie, S. F. Leitman, G. Vilaire, and D. B. Cines. 1983. Inhibition of fibrinogen binding to stimulated human platelets by a monoclonal antibody. *Proc. Natl. Acad. Sci. USA*. 80:2417–2421.
33. Veklich, Y. I., O. V. Gorkun, L. V. Medved, W. Nieuwenhuizen, and J. W. Weisel. 1993. Carboxyl-terminal portions of the alpha chains of fibrinogen and fibrin. Localization by electron microscopy and the effects of isolated alpha C fragments on polymerization. *J. Biol. Chem.* 268:13577–13585.
34. Weisel, J. W., C. Nagaswami, G. Vilaire, and J. S. Bennett. 1992. Examination of the platelet membrane glycoprotein IIb-IIIa complex and its interaction with fibrinogen and other ligands by electron microscopy. *J. Biol. Chem.* 267:16637–16643.
35. Litvinov, R. I., C. Nagaswami, G. Vilaire, H. Shuman, J. S. Bennett, and J. W. Weisel. 2004. Functional and structural correlations of individual αIIbβ3 molecules. *Blood*. 104:3979–3985.
36. Leckband, D. 2000. Measuring the forces that control protein interactions. *Annu. Rev. Biophys. Biomol. Struct.* 29:1–26.

37. Brass, L. F., S. J. Shattil, T. J. Kunicki, and J. S. Bennett. 1985. Effect of calcium on the stability of the platelet membrane glycoprotein IIb-IIIa complex. *J. Biol. Chem.* 260:7875–7881.

38. Litvinov, R. I., G. Vilaire, H. Shuman, J. S. Bennett, and J. W. Weisel. 2003. Quantitative analysis of platelet alpha v beta 3 binding to osteopontin using laser tweezers. *J. Biol. Chem.* 278:51285–51290.

39. Zhu, C., M. Long, S. E. Chesla, and P. Bongrand. 2002. Measuring receptor/ligand interaction at the single-bond level: experimental and interpretative issues. *Ann. Biomed. Eng.* 30:305–314.

40. Cook, B. C. 2001. Reactivity of human platelets with immobilized fibrinogen is dictated by the chemical character of the surface. *Thromb. Res.* 104:39–48.

41. Bell, G. I. 1978. Models for the specific adhesion of cells to cells. *Science.* 200:618–627.

42. Evans, E. 2001. Probing the relation between force-lifetime-and chemistry in single molecular bonds. *Annu. Rev. Biophys. Biomol. Struct.* 30:105–128.

43. Evans, E., and K. Ritchie. 1997. Dynamic strength of molecular adhesion bonds. *Biophys. J.* 72:1541–1555.

44. Lo, Y.-S., Y.-J. Zhu, and T. P. Beebe. 2001. Loading-rate dependence of individual ligand-receptor bond-rupture forces studied by atomic force microscopy. *Langmuir.* 17:3741–3748.

45. Merkel, R., P. Nassoy, A. Leung, K. Ritchie, and E. Evans. 1999. Energy landscapes of receptor-ligand bonds explored with dynamic force spectroscopy. *Nature.* 397:50–53.

46. Boettiger, D., F. Huber, L. Lynch, and S. Blystone. 2001. Activation of α(v)β3-vitronectin binding is a multistage process in which increases in bond strength are dependent on Y747 and Y759 in the cytoplasmic domain of β3. *Mol. Biol. Cell.* 12:1227–1237.

47. Chigaev, A., A. M. Blenc, J. V. Braaten, N. Kumaraswamy, C. L. Kepley, R. P. Andrews, J. M. Oliver, B. S. Edwards, E. R. Prossnitz, R. S. Larson, and L. A. Sklar. 2001. Real time analysis of the affinity regulation of alpha 4-integrin. The physiologically activated receptor is intermediate in affinity between resting and Mn(2+) or antibody activation. *J. Biol. Chem.* 276:48670–48678.

48. Chigaev, A., G. J. Zwartz, T. Buranda, B. S. Edwards, E. R. Prossnitz, and L. A. Sklar. 2004. Conformational regulation of α4β1-integrin affinity by reducing agents: ''inside-out'' signaling is independent of an additive to reduction-regulated integrin activation. *J. Biol. Chem.* 279:32435–32443.

49. Garcia, A. J., J. E. Schwarzbauer, and D. Boettiger. 2002. Distinct activation states of α5β1 integrin show differential binding to RGD and synergy domains of fibronectin. *Biochemistry.* 41:9063–9069.

50. Garcia, A. J., J. Takagi, and D. Boettiger. 1998. Two-stage activation for α5β1 integrin binding to surface-adsorbed fibronectin. *J. Biol. Chem.* 273:34710–34715.

51. Pampori, N., T. Hato, D. G. Stupack, S. Aidoudi, D. A. Cheresh, G. R. Nemerow, and S. J. Shattil. 1999. Mechanisms and consequences of affinity modulation of integrin α(V)β(3) detected with a novel patch-engineered monovalent ligand. *J. Biol. Chem.* 274:21609–21616.

52. Xiao, T., J. Takagi, B. S. Coller, J. H. Wang, and T. A. Springer. 2004. Structural basis for allostery in integrins and binding to fibrinogen-mimetic therapeutics. *Nature.* 432:59–67.

53. Vinogradova, O., T. Haas, E. F. Plow, and J. Qin. 2000. A structural basis for integrin activation by the cytoplasmic tail of the alpha IIb-subunit. *Proc. Natl. Acad. Sci. USA.* 97:1450–1455.

54. Dettmann, W., M. Grandbois, S. Andre, M. Benoit, A. K. Wehle, H. Kaltner, H. J. Gabius, and H. E. Gaub. 2000. Differences in zero-force and force-driven kinetics of ligand dissociation from β-galactoside-specific proteins (plant and animal lectins, immunoglobulin G) monitored by plasmon resonance and dynamic single molecule force microscopy. *Arch. Biochem. Biophys.* 383:157–170.

55. Evans, E., A. Leung, D. Hammer, and S. Simon. 2001. Chemically distinct transition states govern rapid dissociation of single L-selectin bonds under force. *Proc. Natl. Acad. Sci. USA.* 98: 3784–3789.

56. Fritz, J., A. G. Katopodis, F. Kolbinger, and D. Anselmetti. 1998. Force-mediated kinetics of single P-selectin/ligand complexes by atomic force microscopy. *Proc. Natl. Acad. Sci. USA.* 95:12783–12788.

57. Schwesinger, F., R. Ros, T. Strunz, D. Anselmetti, H. J. Guntherodt, A. Honegger, L. Jermutus, L. Tiefenauer, and A. Pluckthun. 2000. Unbinding forces of single antibody-antigen complexes correlate with their thermal dissociation rates. *Proc. Natl. Acad. Sci. USA.* 97:9972–9977.

58. Tees, D. F., R. E. Waugh, and D. A. Hammer. 2001. A microcantilever device to assess the effect of force on the lifetime of selectin-carbohydrate bonds. *Biophys. J.* 80:668–682.

59. Zhang, X., E. Wojcikiewicz, and V. T. Moy. 2002. Force spectroscopy of the leukocyte function-associated antigen-1/intercellular adhesion molecule-1 interaction. *Biophys. J.* 83:2270–2279.

60. Cai, X. E., and J. Yang. 2003. The binding potential between the cholera toxin B-oligomer and its receptor. *Biochemistry.* 42:4028–4034.

61. Schonherr, H., M. W. J. Beulen, J. Bugler, J. Huskens, F. C. J. M. van Veggel, D. N. Reinhoudt, and G. J. Vansco. 2000. Individual supramolecular host-guest interactions studied by dynamic single molecule force spectroscopy. *J. Am. Chem. Soc.* 122:4963–4967.

62. Zhang, X., A. Chen, D. De Leon, H. Li, E. Noiri, V. T. Moy, and M. S. Goligorsky. 2004. Atomic force microscopy measurement of leukocyte-endothelial interaction. *Am. J. Physiol. Heart Circ. Physiol.* 286: H359–H367.

63. Vengasandra, S., G. Sethumadhavan, F. Yan, and R. Wang. 2003. Studies on the protein-receptor interaction by atomic force microscopy. *Langmuir.* 19:10940–10946.

64. Vinckier, A., P. Gervasoni, F. Zaugg, U. Ziegler, P. Lindner, P. Groscurth, A. Pluckthun, and G. Semenza. 1998. Atomic force microscopy detects changes in the interaction forces between GroEL and substrate proteins. *Biophys. J.* 74:3256–3263.

65. Bartolo, D., I. Derenyi, and A. Ajdari. 2002. Dynamic response of adhesion complexes: beyond the single-path picture. *Phys. Rev. E.* 65: 051910.

66. Derenyi, I., D. Bartolo, and A. Ajdari. 2004. Effects of intermediate bound states in dynamic force spectroscopy. *Biophys. J.* 86:1263–1269.

67. Dudko, O. K., A. E. Filippov, J. Klafter, and M. Urbakh. 2003. Beyond the conventional description of dynamic force spectroscopy of adhesion bonds. *Proc. Natl. Acad. Sci. USA.* 100:11378–11381.

68. Hummer, G., and A. Szabo. 2003. Kinetics from nonequilibrium single-molecule pulling experiments. *Biophys. J.* 85:5–15.

69. Bustanji, Y., C. R. Arciola, M. Conti, E. Mandello, L. Montanaro, and B. Samori. 2003. Dynamics of the interaction between a fibronectin molecule and a living bacterium under mechanical force. *Proc. Natl. Acad. Sci. USA.* 100:13292–13297.

70. Savage, B., F. Almus-Jacobs, and Z. M. Ruggeri. 1998. Specific synergy of multiple substrate-receptor interactions in platelet thrombus formation under flow. *Cell.* 94:657–666.

71. Allersma, M. W., F. Gittes, M. J. deCastro, R. J. Stewart, and C. F. Schmidt. 1998. Two-dimensional tracking of ncd motility by back focal plane interferometry. *Biophys. J.* 74:1074–1085.

72. Smith, S. B., Y. Cui, and C. Bustamante. 1996. Overstretching B-DNA: the elastic response of individual double-stranded and single-stranded DNA molecules. *Science.* 271:795–799.